農業工程學報　第41卷第3期
中華民國84年9月出版

Journal of Chinese Agricultural Engineering
Vol. 41. No. 3, September 1995

地下水丘模擬：(Ⅱ). 以Hele-Shaw Model驗證

Simulation of Ground Water Mounding: (Ⅱ). Verification with Hele-Shaw Model

台大水工試驗所博士後副研究員
蔡 存 孝
Tswn-Syau Tsay

美國威斯康辛大學麥迪遜分校土木環工系教授
John Hoopes

摘　要

本文將比較地下水丘在均質與非均質含水層之數質解及由Hele-Shaw模式所得之實驗觀察值，其目的便在驗証此數質模式並測試利用Hele-Shaw模式模擬地下水丘之可行性。Hele-Shaw模式採用SAE 50號機油爲其實驗用液體。實驗與數質模式之結果比較採用均質與含單一矩形異質之含水層，結果顯示實驗與數質解非常一致。但是，當補注量等於模擬之導水係數時，因爲Hele-Shaw模式的空隙已被油所充滿，所以無法觀察出水丘的最高點。

關鍵詞：Hele-Shaw模式，地下水丘。

ABSTRACT

Results of two-dimensional numerical ground water mounding model for a homogereous and non-homogeneous aquifer is compared with observations from a Hele-Shaw model. The purposes of this experiment are to verify the numerical model and test the feasibility of using Hele-Shaw model to simulate ground water mounding. SAE #50 Oil was selected to be used as the experiment fluid in the Hele-Shaw model. Homogeneous aquifer formation was used in the experiments to verify the numerical ground water mounding model. Numerical and experimental results showed good agreement. However, the maximum mounding height could not be observed when the recharge rate was equal to the simulated hydraulic conductivity as the area under the recharge was filled with oil.

Keywords : Hele-Shaw model, Ground water mounding.

1. Literature review and viscous flow analogy

The development of the equations describing flow in a Hele-Shaw model may be found in many places (e. g., Schlichting, 1960; Polubarinova-Kochina, 1962;Harr, 1962; Murray, 1970; and Bear, 1972). The analysis herein follows closely that presented by Bear (1972). The Navier-Stokes equations for a Newtonian fluid with constant density ρ and constant viscosity μ in rectangular coordinates are

$$\rho \frac{D\underline{v}}{Dt} = -\nabla p + \mu \nabla^2 \underline{v} + \rho \underline{g} , \quad \cdots\cdots (1)$$

where $\underline{v}$ is the velocity vector, $\underline{g}$ is the gravitational acceleration vector($= -$ jg with j = unit vector in upward vertical direction), μ ($= \rho \nu$) is the dynamic viscosity and p is the pressure.

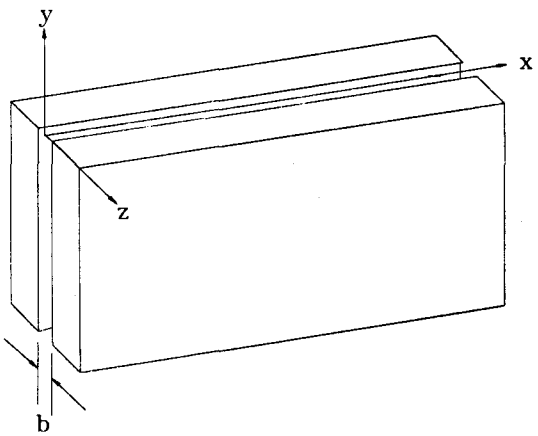

Fig. 1 Coordinate system for derivation of viscous flow analogy equations.

For very slow motions (creeping flow), the inertial term in the equation may be neglected, since the viscous force is dominant. Using the coordinates in Fig. 1, the z-component of velocity vanishes because the flow is parallel to the walls. Hence,

$$0 = -g\frac{\partial \varphi}{\partial x} + \nu \frac{\partial^2 v_x}{\partial z^2} \quad \cdots\cdots (2a)$$

$$0 = -g\frac{\partial \varphi}{\partial y} + \nu \frac{\partial^2 V_y}{\partial z^2} \quad \cdots\cdots (2b)$$

$$0 = \frac{\partial \varphi}{\partial z} , \quad \cdots\cdots (2c)$$

where φ is the piezometric head (p/ γ + y), ν is the kinematic viscosity, and v_x and v_y are velocities in the x and y directions, respectively.Eq. (2c) indicates that φ is constant in the z-direction. As the flow is symmetric about the (x,y) plane

$$\frac{\partial v_x}{\partial z} = \frac{\partial v_y}{\partial z} = 0 \text{ for } z = 0. \quad \cdots\cdots (3)$$

Integrating Eqs. (2a and 2b), using Eq. (3), leads to

$$0 = -gz\frac{\partial \varphi}{\partial x} + \nu \frac{\partial v_x}{\partial z} \quad \cdots\cdots (4a)$$

$$0 = -gz\frac{\partial \varphi}{\partial y} + \nu \frac{\partial v_y}{\partial z} \quad \cdots\cdots (4b)$$

Integrating Eqs. (4a and 4b) from z to b/2 and applying the no slip condition($v_x = v_y = 0$) at $z = \frac{b}{2}$ gives

$$v_x = \frac{g}{2\nu}\frac{\partial \varphi}{\partial x}\left[z^2 - \frac{b^2}{4}\right] \text{ and } \quad \cdots\cdots (5a)$$

$$v_y = \frac{g}{2\nu}\frac{\partial \varphi}{\partial y}\left[z^2 - \frac{b^2}{4}\right] \quad \cdots\cdots (5b)$$

Because of symmetry, Eqs. (5a and 5b) hold for $-\frac{b}{2} \le z \le \frac{b}{2}$. Averaging v_x and v_y over b gives the mean velocities, which are

$$\overline{v_x} = \frac{1}{b}\int_{-\frac{b}{2}}^{+\frac{b}{2}} \frac{g}{2\nu}\frac{\partial \varphi}{\partial x}\left[z^2 - \frac{b^2}{4}\right] dz = -\frac{b^2 g}{12\nu}\frac{\partial \varphi}{\partial x}$$

and $\cdots\cdots (6a)$

$$\overline{v_y} = \frac{1}{b}\int_{-\frac{b}{2}}^{+\frac{b}{2}} \frac{g}{2\nu}\frac{\partial \varphi}{\partial y}\left[z^2 - \frac{b^2}{4}\right] dz = -\frac{b^2 g}{12\nu}\frac{\partial \varphi}{\partial y}$$

$\cdots\cdots (6b)$

If Eqs. (6a) and (6b) are compared to Darcy's law,

$$q = -K\nabla \varphi , \quad \cdots\cdots (7)$$

it is clear that the equivalent hydraulic conductivity, K_m, for the Hele-Shaw (viscous flow analog) is

$$K_m = \frac{b^2 g}{12\nu} \quad \cdots\cdots (8)$$

2. Description of apparatus

The Hele-Shaw model, used in this study, is the one that Murray (1970) built and used for seepage face research. This model, consists of two parallel plates, upst -ream and downstream reservoirs and a motor-transmiss-

ion pump assembly, The two, closely-spaced, plastic (acrylic) plates are one-half inch thick, 30 inches high, and 8 feet long (Fig.2). It was found that a spacing of about 1/10 inch provided a negligible capillary rise (less than 1/10 inch). To facilitate construction, the spacing was designed to be 0.109 inch; 1/8"diameter rods were placed in a square grid (12"x6.5") to help maintain a uniform spacing. On each end of the parallel plates is a reservoir made of 1/2inch acrylic plastic sides, and on the bottom is a 1/2 inch aluminum plate. In order to simulate ground water mounding, recharge is added over a certain protion of the top of the Hele-Shaw model (Fig.3). A peristaltic pump (Fig.4)supplies the constant (and adjustable) recharge rate from the reservoir below the Hele-Shaw model. The recharge flows vertically and freely to the free surface in the model. Hence, the folw rate is equivalent to the hydraulic conductivity (K_m). A flow rate less than K_m is generated by developing a finite, perched aquifer above the water table (Fig. 5). Since the head on the perched aqrifer is not uniform, the recharge rate is not uniform.However, it was shown from this experiment that a uniform recharge (average of the non-uniform pattern from the simulated perched aquifer) yields a good estimate of the ground water mounding.

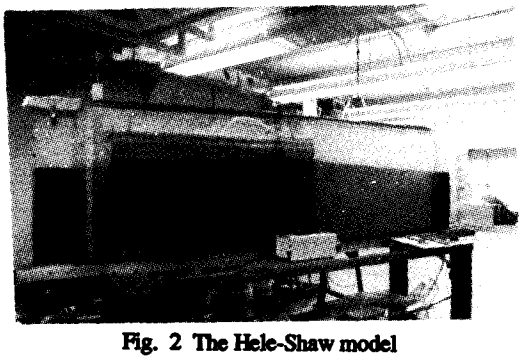

Fig. 2 The Hele-Shaw model

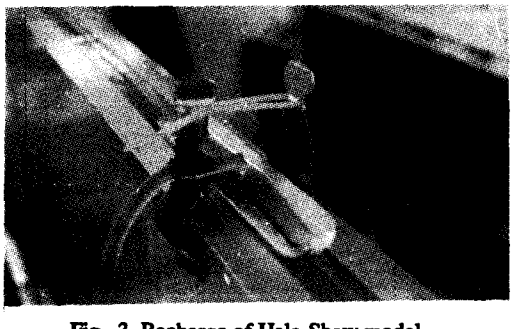

Fig. 3 Recharge of Hele-Shaw model

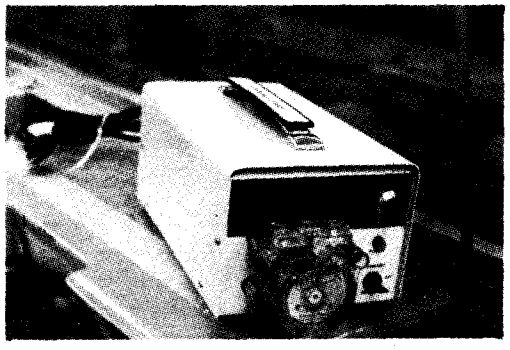

Fig. 4 The peristaltic pump

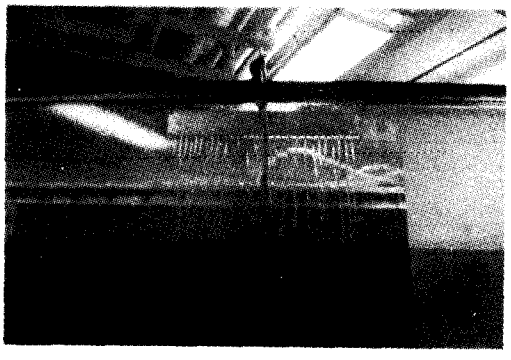

Fig. 5 Perched aquifer for simulating recharge rate less than hydraulic conductivity

3. Selection of experimental fluid and its viscosity

3.1Selection of an experimental fluid

This experiment was to observe the free surface, considerations in the selection of fluid include: (1) fluid kinematic viscosity; (2) sensitivity of viscosity to temperature; (3) surface tension; (4) thermal and chemical stability; (5) Newtonian fluid; and (6) cost.

The fluid viscosity has to be high enough so that the flow is slow enough to neglect the inertial term in the equation of motion (term on left side of Eq.(1)). In addition the fluid has to have negligible capillary effects for the spacing of the Hele-Shaw model. Since the experi-ment was conducted in a temperature controlled room (air-conditioned), the variation of viscosity with temperature can be neglected. According to these considerations, SAE #50 oil was selected amongst glycerin, mineral oil, and various motor oils. It was found that during a test period (2 to 3 hours), no variation in oil temperature was

observed by thermometer. This oil was used in this experiment because of its properites, and it is available and cheap.

3.2Oil viscosity

The viscosity of oil has an inverse relationship with K_m (Eq.(8)), and temperature affects viscosity. In order to find the relation between viscosity of SAE #50 oil and temperature, an experiment was done using a calibrated viscometer (Fig. 6) in a water tank of controlled temperature. The calibrated viscometer is a Canon-Fenske, capillary tube type, size 400, which is good for the fluid viscosity range from 240 to 960 centistokes. The measured relation between viscosity and temperature is shown in Fig. 7. A fitted line, using a second order polynomial, to the experimental data is

$$\nu = 2.838T^2 - 184.014T + 3461.649, \quad \cdots\cdots (9)$$

where T = ℃ and ν = centistokes. The viscosity of the oil ranges from 500-1200centistokes for a temperature range of 17 to 27 ℃ ; thus, K_m ranges from0.6-1.2 cm/sec for the Hele-Shaw model for a spacing of 0.114 inch (calibrated Hele-Shaw model spacing; see next section).

Fig. 6 The viscometer

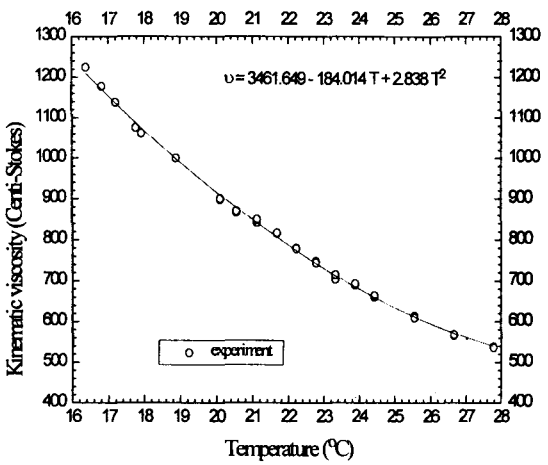

Fig. 7 Relation of viscosity vs. temperature of SAE #50 oil

4. Calibration of Hele-Shaw model spacing

The width, b, between the plates in the Hele-Shaw model was controlled by spacers. An effective "b" was obtained by comparing experimental results with a theoretical solution. Though unconfined flow through a homogeneous aquifer between two reservoirs does not have an exact solution for the free surface,the flow rate is exact. Suppose the constant heads of the left boundary and the right boundary are H_2 and H_1, respectively ($H_2 \cdot H_1$). The flow rate is

$$Q = K_m b \frac{H_2^2 - H_1^2}{2L}. \quad \cdots\cdots (10)$$

Since this is an exact solution, by collecting oil flow from the downstream reservoir and measuring H_2,H_1 and L, K_m can be found by rearranging Eq. (10) as

$$K_m = \frac{2LQ}{(H_2^2 - H_1^2)b}. \quad \cdots\cdots (11)$$

Substituting Eq. (9) into Eq. (11), it follows that

$$b = \sqrt[3]{\frac{24\,\nu\,LQ}{g(H_2^2 - H_1^2)}}. \quad \cdots\cdots (12)$$

Four trials were tested as shown in the following table:

Table 1 Calibration of the Hele-Shaw model spacing

	H_1 (cm)	H_2 (cm)	T (℃)	ν (centistokes)	Q (ml/sec)	b (inch)
Trial 1	41.4	61.2	22.500	758.071	1.080	0.114
Trial 2	41.4	57.7	22.778	742.638	0.878	0.114
Trial 3	41.4	51.1	22.778	742.638	0.483	0.113
Trial 4	41.4	46.8	22.778	742.638	0.259	0.114

According to the trials, the average spacing b is 0.114 inch.

5. Ground water mounding in a homogeneous aquifer

Two simulations were conducted: (1) recharge rate equal to the hydraulic conductivity; and (2) recharge rate less than the hydraulic conductivity.

5.1Recharge rate equal to hydraulic conductivity

Four mounding experiments using the Hele-Shaw model were done to verify the two-dimensional, numerical, ground water mounding model in a homogeneous

aquifer.

The first and second experiments were ground water mounding in a homogeneous aquifer without regional flow, $H_1=H_2$. The third and fourth experiments were ground water mounding in a homogeneous aquifer with regional flow, $H_2>H_1$. The third test had an average regional flow gradient of 9 %, and the fourth test had a regional flow gradient of 7 % ·

These four experiments had a recharge source of width 2w with its center located Lr from the left boundary. The temperature of the oil was T °F. The viscosity of the oil was ν centistokes from Fig. 7. The hydraulic conductivity of the Hele-Shaw model was K_m. The recharge rate, R, was very close to the hydraulic conductivity K_m. The piezometric head of the left and right boundary were controlled to be H_2 and H_1 ,respectively. The data of these four experiments are shown in Table 2. Figs.8a, 9a, 10a, and 11a present the numerical results, which are in very good agreement with the experimental data shown in these figures. Figs. 8b, 9b,10b, and 11b show the grid pattern for the computations. A dense grid was used in the region with high water table curvature, and a sparse grid was used where the water table was flatter. The mass

Table 2 Experimental controlling data of ground water mounding using Hele-Shaw model for Experiment 1, 2, 3, and 4

	Experiment 1	Experiment 2	Experiment 3	Experiment 4
Lr (cm)	130.8	106.0	106.0	106.0
2w (cm)	4.5	6.0	5.0	5.0
T °F	72.3	70.0	68.2	68.2
ν (centistokes)	764	842	909	909
K_m (cm/sec)	0.90	0.81	0.75	0.75
R (cm/sec)	0.90	0.81	0.75	0.75
H_2 (cm/sec)	41.4	41.4	63.7	58.5
H_1 (cm/sec)	41.4	41.4	41.4	41.4

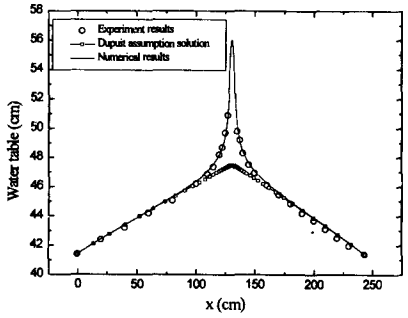

Fig. 8a Comparison of experimental results and numerical results of Experiment 1

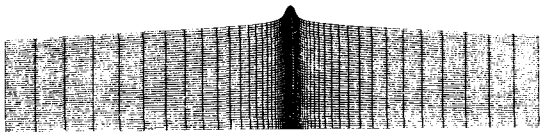

Fig. 8b Grid form for computation of experiment 1

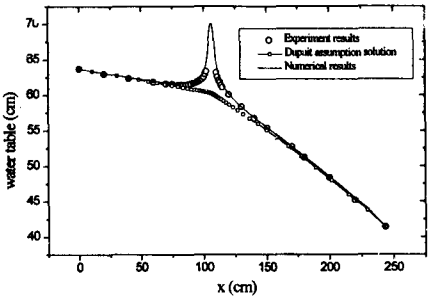

Fig. 9a Comparison of experimental results and numerical results of Experiment 2

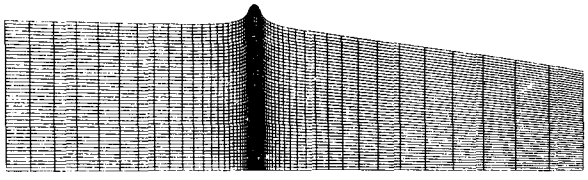

Fig. 9b Grid form for computation of experiment 2

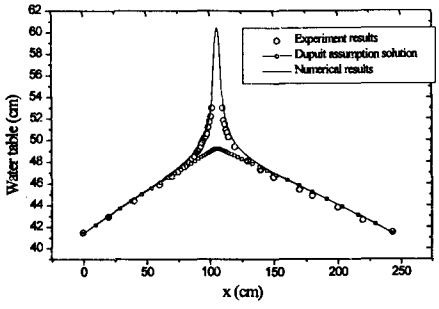

Fig. 10a Comparison of experimental results and numerical results of Experiment 3

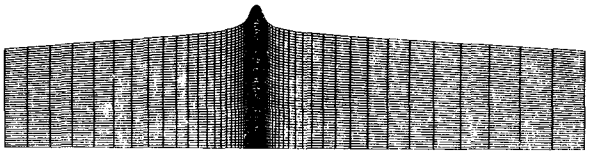

Fig. 10b Grid form for computation of experiment 3

balance error (due to truncation error) was less than 1 % for the simulations.

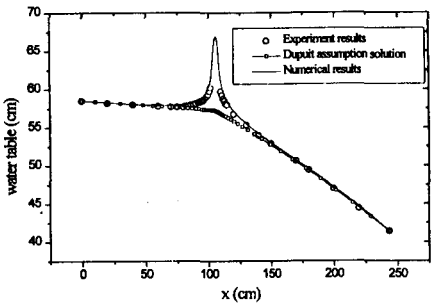

Fig. 11a Comparison of experimental results and numerical results of Experiment 4

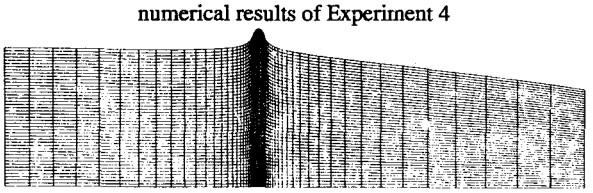

Fig. 11b Grid form for computation of experiment 4

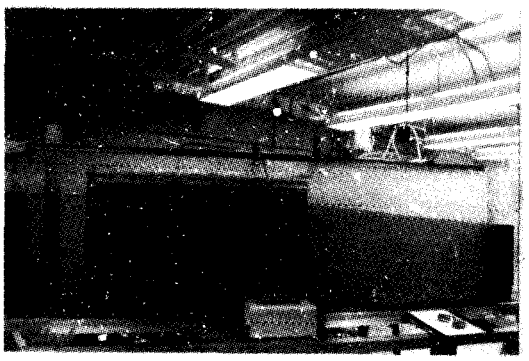

Fig. 12 Ground water mounding when recharge rate equals K_m

The mounding height in the recharge area was not measured because the oil filled the space from the recharge source to the free surface, as shown in Fig. 12.

5.2Recharge rate less than the hydraulic conductivity

Three experiments were done using a perched aquifer to generate a recharge rate less than the hydraulic conductivity (K_m). Experiment 5 had a higher recharge rate than Experiments 6 and 7. The simulation for Experiment 5 does not agree with the observations because the recharge rate distribution is not known as a portion of oil flew off the sides of the perched aquifer.Experiments 6 and 7 closely fit the numerical results. The grid pattern for these three simulations are similar to the four in the previous section. Table 3 shows the experimental data,

Table 3 Experimental controlling data of ground water mounding using Hele-Shaw model for Experiment 5, 6, and 7

	Experiment 5	Experiment 6	Experiment 7
Lr (cm)	109	107.5	107.25
2w (cm)	50	31	30.5
T °F	70	69.5	69.5
v (centistokes)	841.75	859.8	859.8
K_m (cm/sec)	0.813	0.796	0.796
R (cm/sec)	0.088	0.0743	0.0453
H_2 (cm/sec)	41.5	41.5	41.5
H_1 (cm/sec)	41.5	41.4	41.4

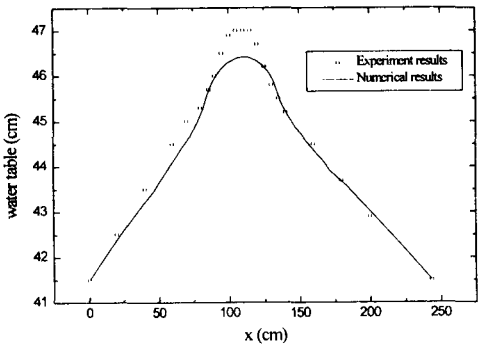

Fig. 13 Comparison of experiment results and numerical results of Experiment 5

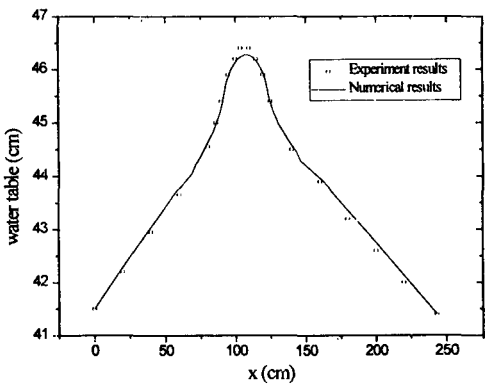

Fig. 14 Comparison of experiment results and numerical results of Experiment 6

and Figs. 13, 14, and 15 are a comparison of the experimental and numerical results.

6.Discussion and conclusions

6.1Differences between numerical and experiment results

As the free surface in the Hele-Shaw model was recorded by eye observation on a scale, there was app-

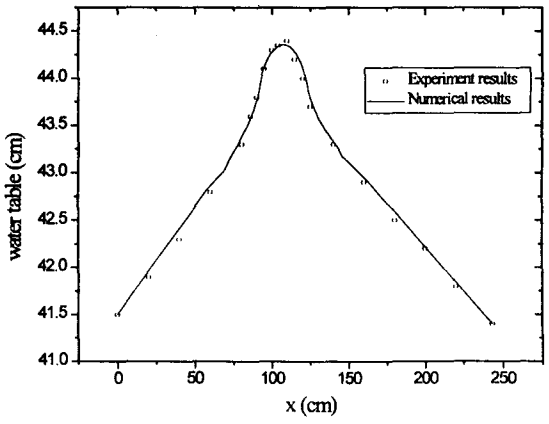

Fig. 15 Comparison of experiment results and numerical results of Experiment 7

roximately a ± 1 mm observation error. The maximum difference and the mean square difference between experiment and numerical results are listed in Table 4.

Table 4 Maximum differece and mean square difference between numerical and experiment results

	Maximum difference (cm)	Mean square difference (cm^2)
Experiment 1	0.56	0.04
Experiment 2	1.18	0.28
Experiment 3	1.28	0.23
Experiment 4	1.46	0.28
Experiment 5	-0.62	0.11
Experiment 6	-0.13	0.01
Experiment 7	0.13	0.004

The maximum differences between numerical and experimental results are around the recharge area, where the free surface gradients are large.

6.2Saturation region above the free surface in the Hele-Shaw model

Mound height below the recharge area can not observed when the recharge rate equals K_m, as shown in Fig. 12. However, numerical results for this experiment showed that there should be a mounding surface under the recharge area. In addition, it was noticed that the recharge width (2w) was not the same from the top of the Hele-Shaw model to the free surface. the recharge width of the top of the Hele-Shaw model for this experiment was larger than that 10 cm below the top of the model by 0.5 cm. This phenomena showed that the recharge (a free flow driven by gravity) was not fully developed until some distance below the top of the Hele-Shaw model (Fig. 16). If the initial free surface is close to the recharge location (top of Hele-Shaw model), a combined flow from recharge and rising of free surface (mounding) happened(Fig. 17). The free surface due to recharge is connected to the top of Hele-Shaw model, and the saturated region is wider than the recharge length. A similar situation happens in ground water if the initial water

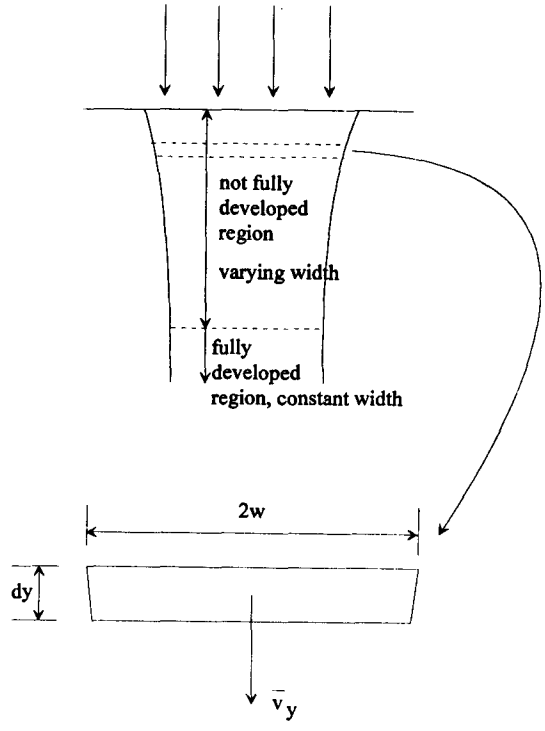

Fig. 16 Development of viscous flow in vertical Hele-Shaw model

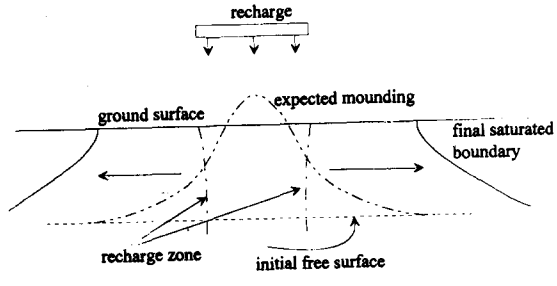

Fig. 17 Conceptual model of ground water mounding when initial free surface close to ground water surface

table is close to the ground surface, the saturated region is much wider than the recharge area.

To determine the minimum distance for a fully developed flow in Fig. 16, assume the pressure in the saturated domain is uniform and equal to atmospheric pressure. Liquid of width 2w by height dy by width b flows at an average velocity v_y (see Fig. 16). Newton's second law requires

$$\rho(2w)(b)(dy)(\bar{v}_y)\left[\frac{d\bar{v}_y}{dy}\right]=\gamma(2w)(b)dy-F_f, \quad (13)$$

where ρ is oil density, γ is oil specific weight and F_f is the friction force. The shear stress on the model walls is estimated by

$$\tau_{yz}=\mu\frac{v_{y,max}}{b/2}=\mu\frac{\bar{v}_y}{b/3} \quad \cdots\cdots (14)$$

so that

$$F_f=2(2w)(dy)\left[\mu\frac{\bar{v}_y}{b/3}\right] \quad \cdots\cdots (15)$$

Substituting Eq. (15) into Eq. (13) gives

$$\frac{\bar{v}_y d\bar{v}_y}{dy}=g-\frac{6\mu}{b^2\rho}\bar{v}_y. \quad \cdots\cdots (16)$$

Integrating Eq. (16) the distance for the fully developed flow is D_f and is given by

$$D_f=-\frac{K_m}{A}-\frac{g}{A^2}\left[ln\left(1-\frac{AK_m}{g}\right)\right], \quad \cdots\cdots (17)$$

where

$$A=\frac{6\mu}{b^2\rho}=\frac{6\nu}{b^2}. \quad \cdots\cdots (18)$$

At 70 °F, ν = 841.75 centistokes = 8.4175 cm^2/sec, K_m= 0.813 cm / sec,b = (0.114x2.54) cm = 0.289 56 cm, and A = 602.3615 sec^{-1} with g = 980cm/sec^2, D_f is 10^{-3} cm from the top of the model which is negligible. Apparently this result does not agree with what's observed. Hence, observation of the recharge stream is necessary.

(A)recharge width observation

Fig. 18 is an observation of the recharge stream in the fully-drained Hele-Shaw model. The total height of the recharge is 70 cm. For a recharge rate 0.944 cm^3/sec, the width in the first (top) 12 cm is 4.8 cm, in the next 10 cm the width is 4.2 cm, and in the last 48 cm the width is 5.5 cm. If the flow has become fully developed after D_f, the width of recharge should be uniform. The varying width observed indicates that the spacing of the plates is not uniform. From Eq. (8), the relation between recharge rate and spacing is

$$\text{recharge rate}=\frac{b^3g(width)}{12\nu}, \quad \cdots\cdots (19)$$

which gives the spacing of these three sections to be 0.114 inch, 0.119 inch and 0.109 inch, respectively, These values are very close to the results in Table 6.1. Hence, the varying width probably caused by the non-uniform spacing. At a temperature of 66 OF, ν = 998.4 centistokes, which means that K_m= 0.69cm/sec, 0.75 cm /sec and 0.63 cm/sec for the three sections of the recharge stream, respectively, The average value of K_m is 0.69 cm/sec.

(B)observation of flowing speed

From Eq. (5b), the velocity profile in the y-direction is parabolic. The maximum velocity at z = 0 is

$$v_{y,max}=\frac{g}{2\nu}\frac{\partial\varphi}{\partial y}\left[-\frac{b^2}{4}\right]; \quad \cdots\cdots (20)$$

Eq. (6b) gives the average velocity as

$$\bar{v}_y=\frac{2}{3}v_{y,max}. \quad \cdots\cdots (20)$$

Three small air bubbles in the recharge stream center were observed. The time for these bubbles to move a distance of 6 inches was 13.85 sec, 16.57 sec and 15.91 sec, respectively, giving an average velocity of the

Fig. 18 Recharge in a fully drained Hele-Shaw model

(文轉第 77 頁)